Supplementary Information for

Tubulin Tails and their Modifications Regulate Protein Diffusion on Microtubules

Lavi S. Bigman and Yaakov Levy*

Yaakov Levy
Koby.Levy@weizmann.ac.il

This PDF includes:

- Supplementary text
- Figs. S1-S9
- Legends for movies M1-M4
- References for SI citations

Methods

Model generation

To study the diffusion of proteins along MTs, we constructed an MT lattice consisting 4 protofilaments each consisting of 3 heterodimeric tubulin molecules (i.e., the lattice includes 6x4 monomeric tubulin proteins). The coordinates of the MT lattice were based on the structure of a single isoform neuronal human MT (PDB ID 5JCO) (1). The disordered tails (residues 438–451 of α tubulin and 427–450 of β tubulin) were added as linear chains to the C-terminal of each tubulin monomer. A more realistic conformation of the tails was obtained by the simulations (see below).

In this study, we chose to study MT bearing tails of isoform α1A and β3, which comprise 14 and 24 residues, respectively. The sequences of the tubulin tails are DSVEGEGEEEGEEY for α tubulin (isoform α1A, net charge of -8) and DATAEEEGEMYEDDEEESEAQGPK for β tubulin (isoform β3, net charge of -11). The underlined Glu served as the PTM site. The diffusing proteins used in this study are MT binding domains of EB1 (residues 1-130, pdb ID 1PA7) PRC1 (2) (residues 341-464, pdb ID 5KMG) and Tau (3) (residues 256-267, PDB ID 6CVJ).

Coarse-grained molecular dynamics simulations

The dynamics of protein diffusion along MTs was studied using coarse-grained molecular dynamics simulations that enable the investigation of long-time scale processes that are challenging for high-resolution models. Each residue was represented by a single bead at the position of its Cα atom.

The force-field applied in our simulations used a native-topology based model that includes a Lennard-Jones potential to reward native contacts and a repulsive potential to penalize to non-native contacts (4–6). Electrostatic interactions between charged residues were modeled using the Debye-Hückel potential (7). The explicit form of the force field is:

$$
\begin{aligned}
V(\Gamma,\Gamma_0) = & \sum_{bonds} K_{bonds}\left(b_{ij}-b_{ij}^0\right) + \sum_{angles} K_{angles}\left(\theta_{ijk}-\theta_{ijk}^0\right) \\
& + \sum_{dihedrals} K_{dihedrals}\left(\left[1-\cos\left(\varphi_{ijkl}-\varphi_{ijkl}^0\right)\right] + \frac{1}{2}\left[1-\cos\left(3\left(\varphi_{ijkl}-\varphi_{ijkl}^0\right)\right)\right]\right) \\
& + \sum_{i\neq j} K_{contacts}\left[5\left(\frac{A_{ij}}{r_{ij}}\right)^{12} - 6\left(\frac{A_{ij}}{r_{ij}}\right)^{10}\right] \\
& + \sum_{i\neq j} K_{repulsions}\left(\frac{C_{ij}}{r_{ij}}\right)^{12} + \sum_{i\neq j} K_{electrostatics} B(\kappa) q_i q_j \frac{e^{-\kappa r}}{\varepsilon_r r_{ij}}
\end{aligned}
$$

where K_{bonds}=100 kcal mol^{-1} Å^{-2} ,K_{angles}=20 kcal mol^{-1}, and $K_{dihedrals}$, $K_{contacts}$, $K_{repulsion}$ are each valued at 1 kcal mol^{-1}. The term b_{ij} is the distance (in Å) between bonded beads *i-j*, and b^0_{ij} is the optimal distance (in Å) between bonded beads *i-j*. The term θ_{ijk} is the angle (in radians) between subsequentially bonded beads *i-j-k* and θ^0_{ijk} is the optimal angle between subsequently bonded beads *i-j-k*. The term φ_{ijkl} is the dihedral angle (in radians) between subsequently bonded backbone beads *i-j-k-l* and φ^0_{ijkl} is the optimal dihedral angle between subsequently bonded backbone beads *i-j-k-l*. A_{ij} is the optimal distance (in Å) between beads *i-j* that are in contact with each other and r_{ij} is the distance (in Å) between beads *i-j* in a given conformation along the trajectory. Optimal values were calculated from the atomic coordinates of the structures. C_{ij} is the sum of radii for any two beads not forming a native contact; the repulsion radius of the backbone bead was 2.0 Å. The last term in the force field is the Debye-Hückel potential, where $K_{electrostatics}$= 332 kcal Å mol^{-1} e^{-2}, $q_{i/j}$ is the sign of the charged residue, ε_r is the dielectric constant, κ is the screening factor, B(κ) is the salt-dependent coefficient, and r_{ij} is the distance (in Å) between charged residues i and j. We point out that, because of the coarse-grained representation of the systems, the effective salt concentration may correspond to a higher value (by a factor of ~3) than for an atomistic representation. More details regarding the Debye-Hückel potential can be found in ref (7).

In order to reduce computational time, electrostatic interaction between the diffusing proteins and charged residues of both α and β tubulin that are located at the interior of the microtubules were eliminated. This elimination did not affect the properties of the MT surface, which is relevant to the diffusion process. Hydrophobic interactions were not included in our model, since the distribution density of hydrophobic residues on the surface of EB1, tubulin and tubulin tails is much lower than the distribution density of charges residues (Fig. S1). Yet, one may expect that hydrophobic interactions between the diffusing protein and the MT will slow down the diffusion.

The beads of the structured part of the MT (referred to herein as "MT body") were kept fixed in our simulations but the tails were flexible. Avoiding internal flexibility for the folded domains of the MT is a reasonable assumption given the rigidity of MT structures and avoids deformation of the MT slice used in our summations. Furthermore, the internal dynamics of the tubulin monomers is not expected to contribute to diffusion on MT. The flexibility of the disordered tubulin tails was controlled by its bond and dihedral angles.

The dynamics of protein diffusion along MTs were simulated using the Langevin equation. The simulation temperature was set to 0.4 (reduced units), which is lower than the folding temperature of EB1 or PRC1. The Tau protein is intrinsically disordered and was simulated at the same temperature for consistency. The dielectric constant was 80, and the salt concentration was 0.02 M unless stated otherwise. The system was confined in a box of dimensions 350×400×330 Å, and the longitudinal direction of the MT was aligned along the Y-axis. For all the systems, we preformed 50 simulations consisting of $2*10^7$ essential MD steps. Trajectory frames were saved every 1000 steps. Periodic boundary conditions were not used in our model.

We preformed also simulations with $5*10^7$ essential MD steps, to test if increasing simulation time improves the sampling of the MT lattice in each independent repeat. Comparing the MSD plots and diffusion coefficients calculated from long and short simulations with similar accumulated times revealed no significant difference between the two (Fig. S9). We note that estimating D from MSD might be affected by the finite size of the system, such that the maximum displacement is bounded, however, in the timescale of the performed simulations the lattice that was used was large enough. The similar D values from the short and long simulations runs confirm that.

Systems with modified charges

To study the contributions to protein diffusion along MT that arise from the electrostatic potential of the tubulin folded domains, the tail, and cross-talks between them, we constructed several variants of MT where the charges of the body or of the tail residues were modified. Several series of variants were designed to dissect the effect of MT electrostatics on the diffusion of MT-binding proteins. The following series were designed:

1. Neutral α/β tail: In this series, the charges of the α, β, or both α and β tail were removed. In these variants the MT body retains its wild-type charges.
2. All α or β tail: In these variants, the α tail was replaced by a β tail to generate an all-β tail tail, and vice versa to generate an all-α tail tail. In these variants, the MT body retains its wild-type charges.
3. Modified α/β tails: In these variants, the charges of the α and β tail are successively titrated while the charges of the folded domains remain invariant.
4. Neutral body and modified α/β tail: In this series, the charges of all MT body residues were neutralized and the charges of the tails were titrated gradually. In this series, the "pseudo wild-type" variant includes all the charges of the tails (*i.e.*, net

charge of -8 and -11 for the α and β tails). The variants were designed by successively neutralizing the charges on the tail residues, two from each tail per variant. In these variants, thus, the total net charges of the α and β tail were -19, -14, -10, -6, -2 and 0. Some of these variants are discussed in Figure 4A.

5. Neutral body, neutral β tail, and modified α tail: In this series of variants, both the folded domains and the β tail are completely neutralized electrostatically so only the α tail bears charged residues. The variants were constructed by successively neutralizing two negative charges from the α tail, resulting in variants with net charges on the α tail of -8, -6, -4, -2, and 0. These variants are discussed in Figure 4C.
6. Neutral body, neutral α tail, and modified β tail: In this series of variants, both the folded domains and the α tail are completely neutralized electrostatically, so only the β tail has charged residues. The variants were constructed by successively neutralizing two negative charges from the α tail, resulting in variants with net charges on the α tail of -11, -9, -7, -5, -3, -1 and 0. These variants are discussed in Figure 4D.
7. Neutral body and neutral α/β tails: in this series, the charges were removed from both α and β tail residues. The variants were designed by changing the magnitude of the charges of the folded domains. Whereas, in the "pseudo wild type" variant, the charged residues are $q = \pm 1$ for positively or negatively charged residues, in the other variants the charges vary from 0.2 to 2.2. These variants are discussed in Figure 4B.

Systems with PTMs

The effect of polyglutamylation or polyglycylation on protein diffusion along MT was studied by modifying the tail through the addition of polyE or polyG chains, respectively. The polyE/G chains were added by creating a peptide bond between the amino terminal of the chains and the C_γ atom of glutamate 445 in α tubulin or glutamate 435 in β tubulin. These sites were previously identified as common positions for polyglutamylation (8–10) and were used as polyglutamylation sites to study the effect of polyE on the activity of motor proteins (11). We constructed CG systems with 5, 10, 15, and 20 residue polyE/G chains branched off the α and β tails.

All-atom molecular dynamics simulations

To complement the CG model, we also preformed all-atom simulations, which were performed on a smaller "slice" of MT consisting of 3 protofilaments, each consisting of 2 heterodimeric tubulin (i.e., the lattice includes 3x4 monomeric tubulin proteins). The initial conformation for the all-atom simulation was based on the same structure as the CG model (PDB ID 5JCO), and the tubulin tails were again modeled as linear chains but demonstrated a large conformational heterogeneity during the simulation (see SI Fig. 2). The atomistic simulations were performed for the MT lattice in order to quantify the conformational dynamics of the tails. In addition, simulations were performed on MT with EB1, to examine the interactions between EB1 and the MT body and disordered tails.

The simulations were performed using GROMACS (12) version 2018.3. The molecular system was solvated in a box with periodic boundary conditions containing pre-equilibrated SPC/E water molecules. Na^+ and Cl^- ions were added to maintain overall system neutrality with salt concentration of 0.125 mM. We used the AMBER99SB-ILDN (13) force field . The LINCS algorithm (14) was used to control bonds during the simulation. The leapfrog algorithm was employed with steps of 2 fs. Temperature was controlled at 300 K using a modified scheme of the Berendsen thermostat (15). The system was minimized using the steepest descent algorithm. Next, the system was equilibrated under an NVT ensemble and an NPT ensemble (100 ps each phase). Production runs were executed at constant pressure (1 atm). During production runs, the Cα atoms of the MT body residues were kept fixed to prevent lattice distortion and to enhance computation performance.

The above steps were applied both for a system including only MT and for a system that included EB1 and MT. We preformed 5 repeats of 500 ns runs for each system on the PizDaint supercomputer at the Swiss National Supercomputing center, utilizing multiple GPU nodes in parallel. For the systems with EB1, the starting position of EB1 was different in each repeat.

Trajectory Analysis

Calculation of diffusion coefficients

The trajectories from the CG simulations (Fig. S7 and S8) were analyzed using in-house scripts. The mean square displacements (MSD, Fig. S9) of the proteins center of mass (COM) was calculated using the equation:

$$MSD(\tau) = \sum_{i=t_0}^{t-\tau} \frac{(r_{i+\tau} - r_i)^2}{t-\tau} = 2dD\tau$$

Where *r* is the position of the protein COM, t is the number of time steps measured, and τ is the measurement window ranging from t_0 to t. The slope of MSD is 2d*D*, where d is the dimensionality of diffusion and *D* is the diffusion coefficient, which was calculated between time frames 1500 and 3000, since shorter time scales do not capture the slow diffusion process. We calculated diffusion along protofilaments (longitudinal diffusion, D_y) and across them (lateral diffusion, D_x), hence d=1in all the calculations used in this study.

Diffusion coefficients were calculated also using a kinetic analysis. In each trajectory we measured the transition time for 8 nm steps along the protofilament axis (y axis in Fig. S7 and S8) (size of tubulin dimer). The transition times were averaged and converted to diffusion coefficients using: $D = a^2/2\tau$, where a is the step size (a=8 nm in our case) and τ is the corresponding transition time (Fig. S6). The distribution of D values is similar for kinetic based and MSD based calculations, although the average values from the kinetic analysis are higher by up to a factor of 5, depending on salt concentration (Fig. S4). Note also that the D values from MSD based calculations are closer to the experimental values.

Estimation of energy barriers from potential of mean force

Change in the free energy landscape of EB1 diffusing on MT when varying the charge of the MT tail and body (Fig. 4), was extracted from the potential of mean force (PMF) of the position of EB1 along the x and y axis of the MT. PMF was calculated by $PMF=-\log(p_i)$, where p_i is the probability of EB1 to be in a the i^{th} bin along the x or y axis of the MT. PMF_y was calculated from configurations in which the x position of EB1 was between -50 to 50 Å. PMF_x for systems with neutral body and neutral tails (Fig. 4A and 4B) was calculated from configurations in which the y position of EB1 was between -80 to 80 Å. For the system with neutral α tails or neutral β tails, PMFx was calculated from configurations in which the y position of EB1 was between -80 to 0 Å or -40 to 40 Å, respectively.

Calculation of fraction of bound conformations to MT, MT body and tubulin tails

Bound conformations were defined as conformations in which the protein was bound to the MT, e.g., the proteins COM was less than 50 Å above the MT surface, and within the horizontal and vertical boundaries of the MT lattice. The fraction of bound conformations was defined as:

$$f(bound) = \frac{N_{bound}}{N_{total}}$$

Where N_{bound} is the number of bound conformations and N_{total} is the total amount of conformations in the simulation. We note that the MSD was calculated only for the bound conformations.

In Figure 5, the fraction of conformations in which EB1 was bound to the MT body or to tails was based on the electrostatic interaction energy between the protein residues and tail/body residues. The protein was defined as bound to the MT body if the protein–MT body interaction, $E_{prot\text{-}body}$<=-0.03 $kcal \cdot mol^{-1} \cdot atom^{-1}$ and protein–tail interaction energy $E_{prot\text{-}tail}$ >=-0.04 $kcal \cdot mol^{-1} \cdot atom^{-1}$. The protein was defined as bound to the MT tails if $E_{prot\text{-}body}$>0.03 $kcal \cdot mol^{-1} \cdot atom^{-1}$ and protein–tail interaction energy $E_{prot\text{-}tail}$ <-0.04 $kcal \cdot mol^{-1} \cdot atom^{-1}$. Thereafter, the fraction bound to body/tail was calculated by:

$$f(tail/body) = \frac{N_{tail/body}}{N_{total}}$$

Where $N_{tail/body}$ is the number of tail/body bound conformations and N_{total} is the total amount of conformations in the simulation.

Validation of tail properties in CG simulations

The properties of tubulin tails in the CG simulations were validated against all-atom simulations by measuring three properties of the tubulin tails: Radius of gyration (Rg), the vertical angle (denoted θ, Fig. S2 A) between the tubulin tails and the MT lattice and the lateral displacement (denoted ϕ) of the tubulin tails with the plan of the MT.

Rg was measured based on the Cα atoms of the tails of α (residues 438–451) and β (residues 427-450) tubulin.

In order to calculate the mentioned angles, we define several vectors:

1. $\mathbf{v_{a/b}}$ is the vector connecting the first (D438/D427) and last (Y451/K450) residues of α/β tails,
2. $\mathbf{p1_{\alpha/\beta}}$ is the vector connecting the first residue of α/β (D438/D427) and the first residue of β/α tail (D427/D438)
3. $\mathbf{p2_{\alpha/\beta}}$ the vector connecting the first residue of two adjacent α/β tails (D438).

Since $p1_{\alpha/\beta}$ and $p2_{\alpha/\beta}$ both reside in the MT plane, we can define the MT plane by its normal:

$$Np_{\alpha/\beta} = \boldsymbol{p1}_{\boldsymbol{\alpha/\beta}} \times \boldsymbol{p2}_{\boldsymbol{\alpha/\beta}}$$

And then θ is the angle between α/β tail and the MT plane defined as:

$$\theta = 90 - \tan^{-1}\left(\frac{\sin(V_{\alpha/\beta} \cdot Np_{\alpha/\beta})}{\cos(V_{\alpha/\beta} \cdot Np_{\alpha/\beta})}\right) \quad \text{[Eq. S1]}$$

ϕ is the angle between the projection of the tubulin tail on the MT plane and $\mathbf{p1_{\alpha/\beta}}$.
These properties were measured in both atomistic and CG simulations.

Diffusion of PRC1 and Tau on MTs

Diffusion of PRC1 and Tau was studied under different salt concentrations on three types of MT lattice: 1) MT with the wild-type tails of both α and β tubulin (see *SI Methods* for exact definition) 2). MT without α/β tails, 3) MT tails modified by the addition of poly-glutamate (polyE) chains that were 10 amino-acids long. Similar to EB1 (Fig. S3 top row), increasing salt concentration leads to a gradual increase in the diffusion coefficient (*D*) in systems with no tails (Fig. S3 second and third row, blue circles) or with WT tails (red circles), and to a less significant increase for systems with polyglutamylated tails (orange circles). The lateral diffusion coefficients (D_x) for EB1, PRC1 and Tau were also calculated (Fig. S3, middle column). Increasing the ionic strength also leads to increased dissociation events for PRC1 and Tau from the MT and therefore the fraction of PRC1 and Tau bound to MT decreases (Fig. S3, third column color code same as Fig. S3 columns 1 and 2).

Validation of tail properties in CG simulations

In order to increase the reliability of our CG model, the force parameters of tubulin tails in the CG model were validated against all-atom simulations. For both types of simulation, we measured the radius of gyration (Rg) of the α and β tubulin tails, the vertical angle (denoted θ, Fig. S2A, left) between the tubulin tails and the MT lattice and the lateral displacement (denoted ϕ, Fig. S2A, right) of the tubulin tails within the MT plain (See *SI Methods* and Fig. S2 for detailed description). In Fig. S2 we show the distribution of Rg, (panel B) θ (panel C) and ϕ (panel D) for α (red) and β (magenta) tubulin tails for atomistic (dashed line) and CG (solid line) simulations. When the CG model included only bonded and electrostatic terms for tail residues, the distributions for all three properties were similar for both all-atom and CG simulations.

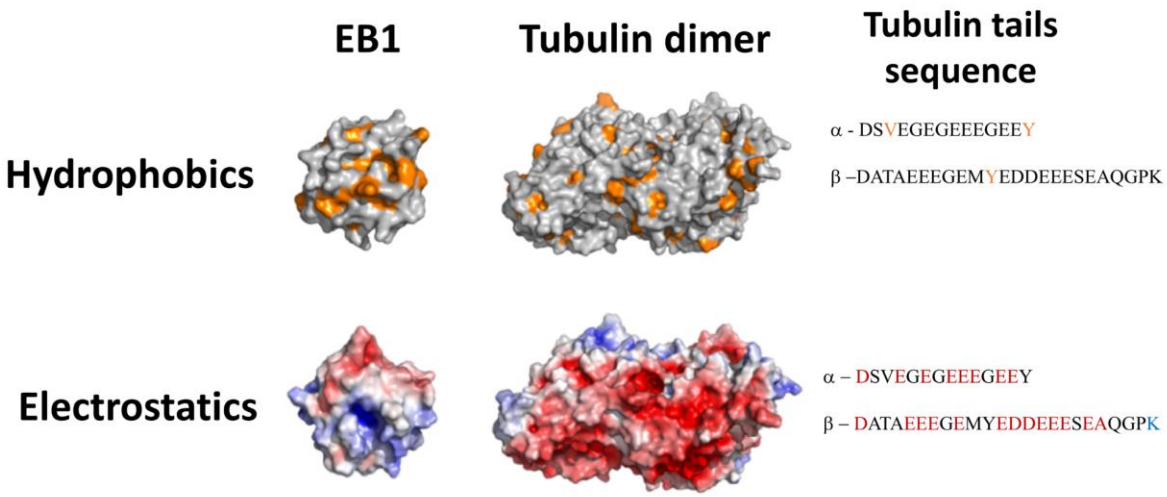

Figure S1. Distribution of charged and hydrophobic residues on EB1 and tubulin. Hydrophobic residues are shown in orange, non-hydrophobic in gray for EB1 and tubulin heterodimer. Electrostatic potential mapped onto the surface of the proteins are marked by red and blue. The hydrophobic and charged residues are also marked on the sequences of α and β tubulin tails used in this study. Hydrophobic residues are colored in orange, positively and negatively charged residues are shown in blue and red, respectively. Electrostatic potential maps were calculated using the APBS (18) plugin in PyMOL©. Hydrophobic residues are: valine, isoleucine, leucine, tryptophan, phenylalanine and tyrosine.

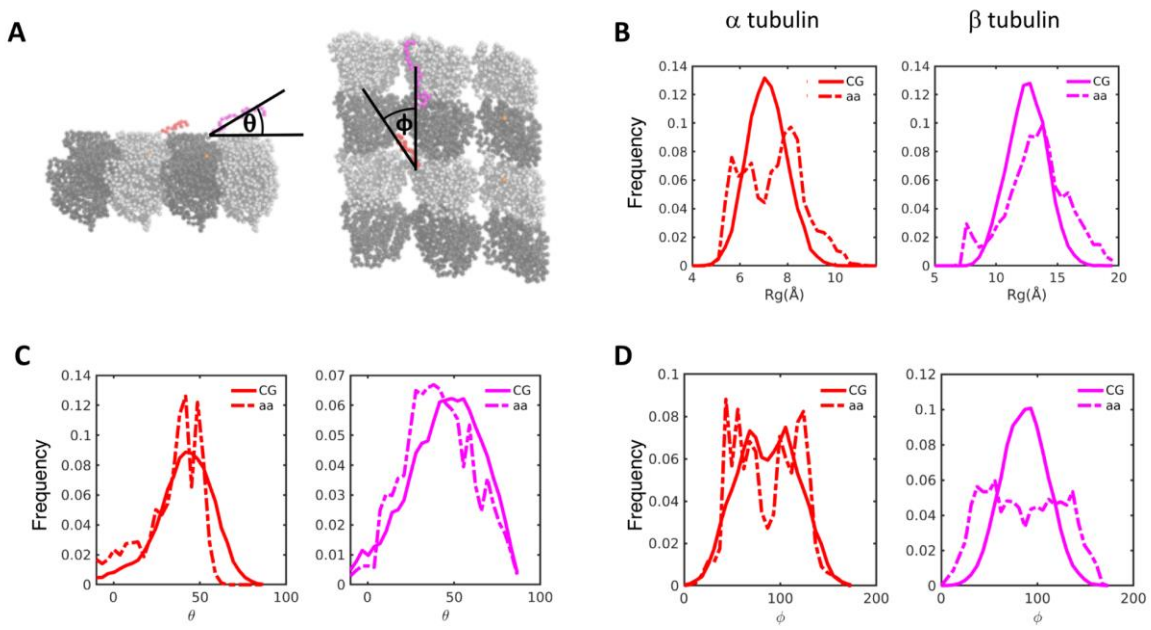

Figure S2. Validation of tail properties in CG simulations. (A) Left - The vertical angle θ between tubulin tails and the plane of the MT lattice. (See SI Methods for detailed description). Right - The lateral displacement of α (red) and β (magenta) tubulin tails is measured by the angle ϕ, defined as the angle between the projection of the tubulin tail on the MT lattice and the vector connecting the first residue of α and β tubulin (See SI Methods for detailed description). (B) The distribution of radius of gyration of α (red) and β (magenta) tubulin tails is shown for all-atom (dashed line) and CG simulations (solid line). (C) The distribution of the vertical displacement θ of tubulin tails. (D) Distribution of lateral displacement f of tubulin tails. The key in C and D is the same as in B.

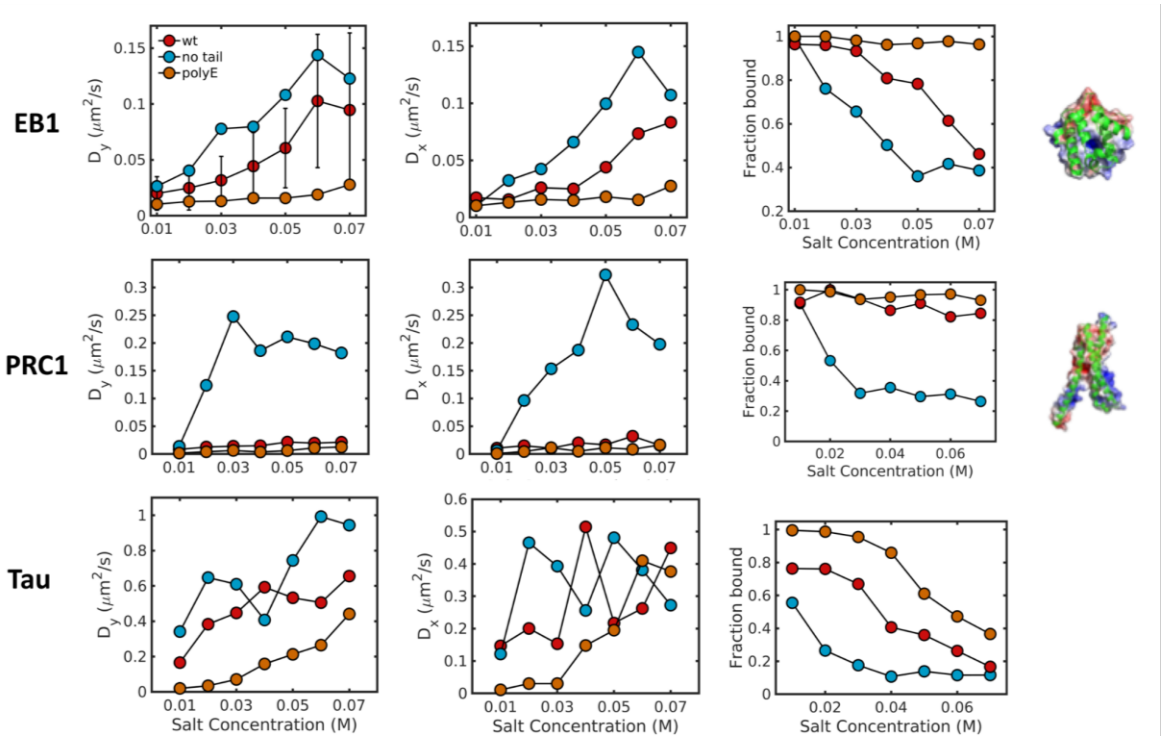

Figure S3. Diffusion of PRC1 and Tau on MTs. First column: Diffusion of EB1(first row), PRC1(second row) and Tau (third row) as a function of salt concentration on MT lattice with WT tails (red circles), no tails (blue circles) and polyglutamylated tails (orange circles). Second column: Same as first column, but for lateral diffusion of the proteins. Third column: The fraction of time EB1, PRC1 and Tau are bound to the MT lattice as a function of salt concentration for MT lattice with different tail properties. Color code is the same as in the first column.

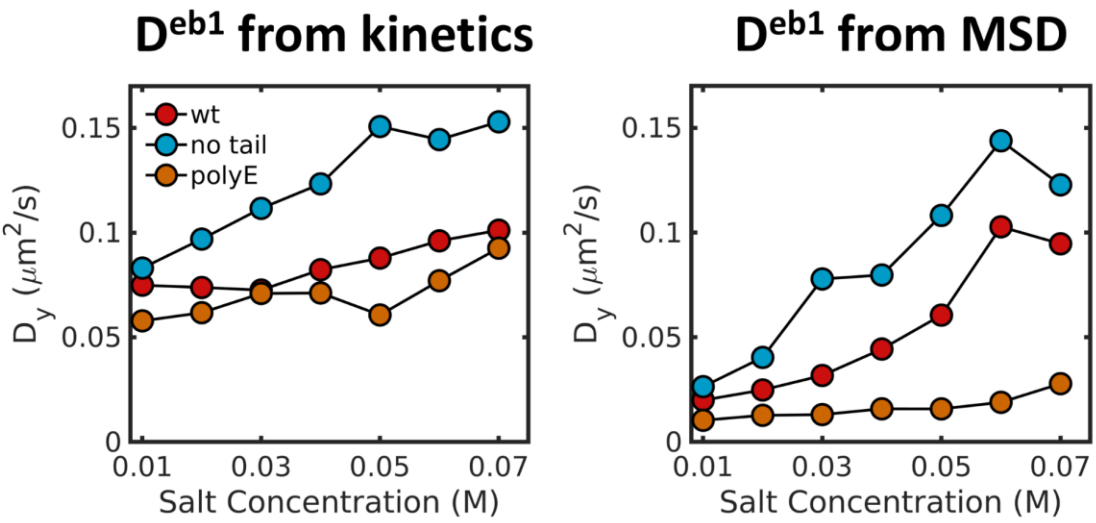

Protein	D_y MSD (μm²/s)	Dy Kinetics (μm²/s)	Experiment (μm²/s)
Tau	0.44±0.25	0.46±0.35	0.29
EB1	0.03±0.02	0.14±0.09	0.019± 0.005
PRC1	0.014±0.006	0.05±0.01	0.039± 0.005

Figure S4. Comparison of diffusion coefficients from MSD analysis and kinetic analysis. (Left) Diffusion coefficient as a function of salt concentration, calculated using kinetic analysis. Color code indicated on the figure. (Right) Diffusion coefficient as a function of salt concentration, calculated using MSD analysis. The dependency of D_y on salt concentration is similar for kinetic and MSD analysis, although the values obtained from kinetic analysis are slightly higher. (Bottom table) Diffusion coefficients of the proteins used in this study calculated by MSD analysis, kinetic analysis, and experimental data (16, 17). The values shown in the table were calculated for a system with WT MT at salt concentration of 0.03 M. Errors represent standard deviation.

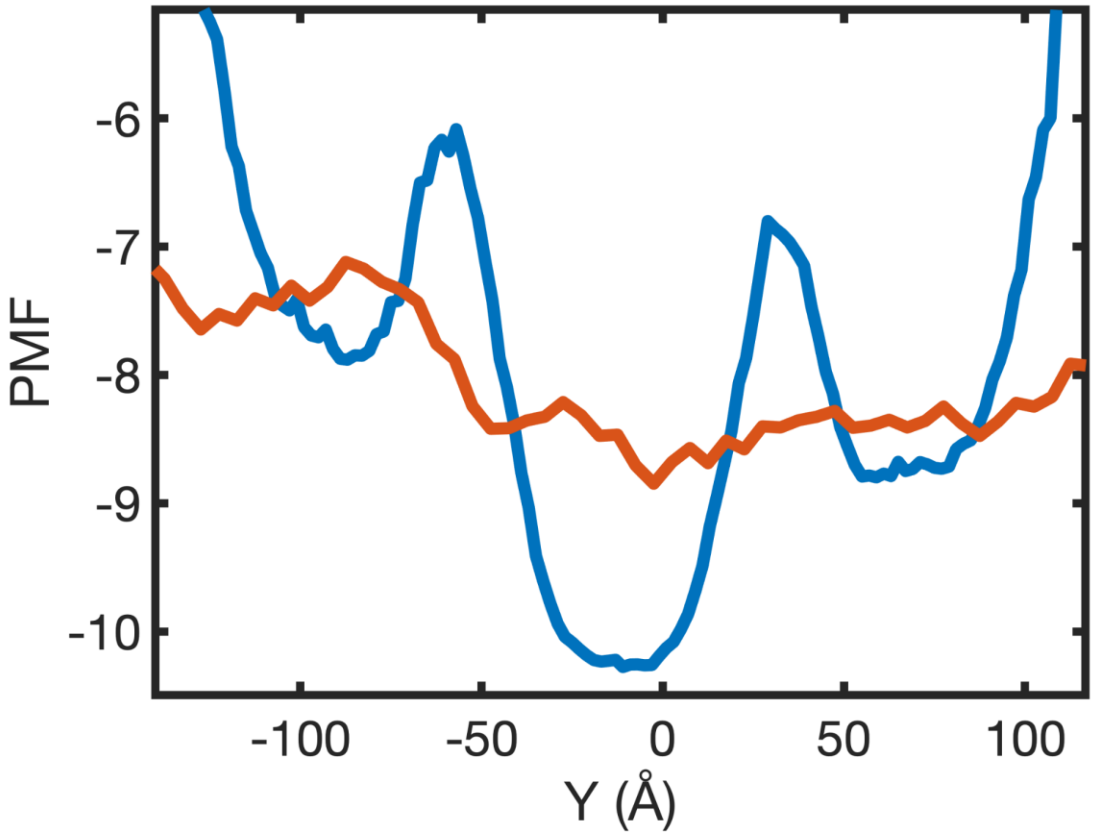

Figure S5. Ruggedness of energy landscape is negligible in comparison to energy barrier. The potential of mean force (PMF) is shown projected along the y coordinate of EB1 diffusing on MT. The blue line is the PMF of tail mediated diffusion, where both α and β tails are charged, and the red line is the PMF when the tails where fully neutralized. With charged tails there is a clear energy barrier for hopping between position ~0 to ±80, while for the system with neutral tails the barrier diminishes, although the PMF is still rugged.

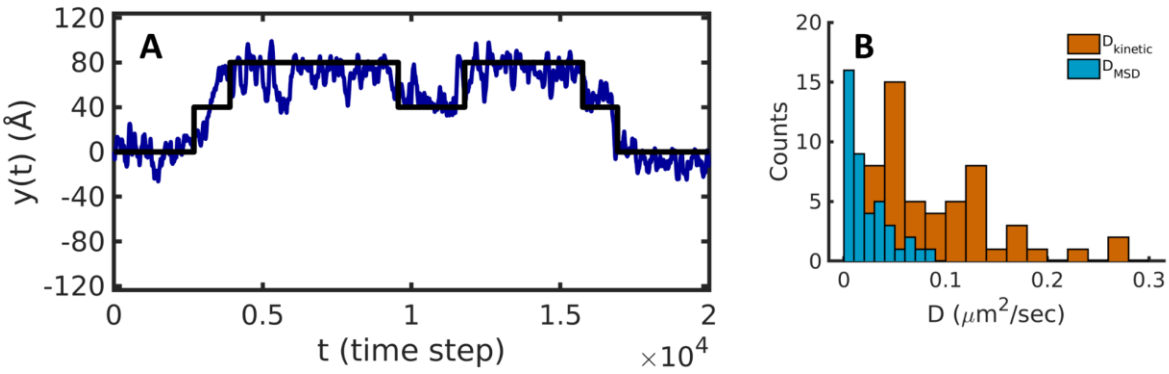

Figure S6. Extracting diffusion coefficients from kinetic analysis of the trajectories. (A) Representative trajectory of EB1 diffusing on WT MT (blue line). The black line shows the discrete hops of EB1 on the MT lattice. From each trajectory we calculated transition times for hopping of 8 nm, which is the size of tubulin dimer. (B). Histograms of diffusion coefficients extracted of MSD analysis (blue bars) and kinetic analysis (orange bars). Note the distributions of D values are similar for both types of analysis, although the values obtained from the kinetic model are higher.

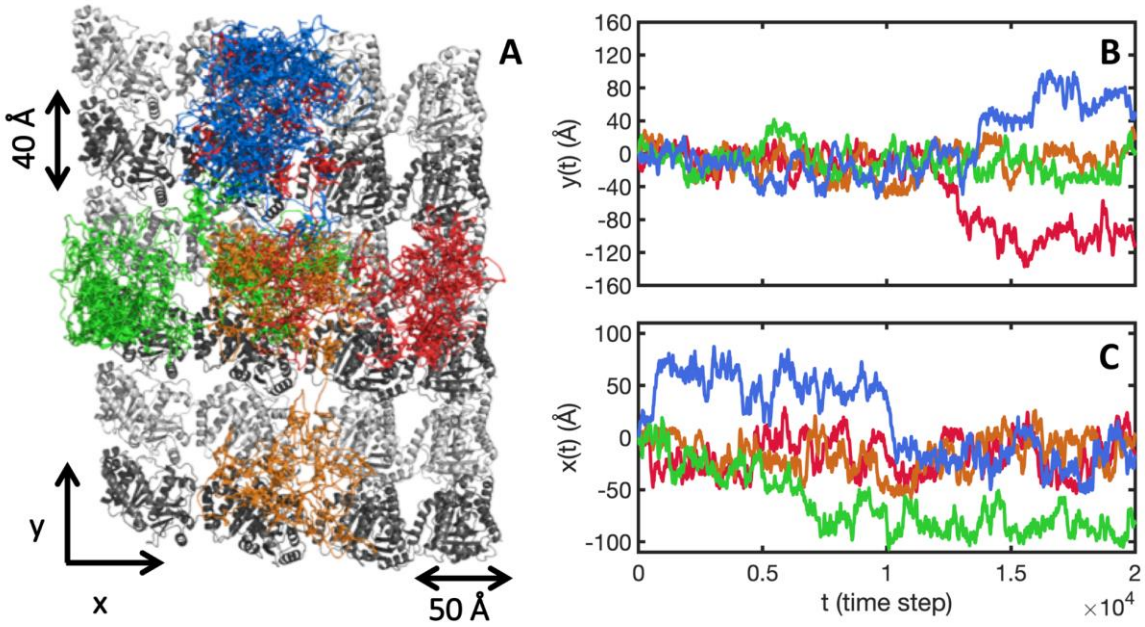

Figure S7. Trajectories of EB1 diffusing on WT MT. (A) Location of center of mass of EB1on a WT MT lattice. We show here trajectories from 4 independent simulation runs, each in a different color. (B) Location of center of mass of EB1 along the y axis as a function of time for the same trajectories shown in panel A. Note hops of 4 and 8 nm, which are the size of tubulin monomer and dimer, respectively. (C) same as B, but for the x coordinate. Notice jumps of 5 nm, which is the size of a side step.

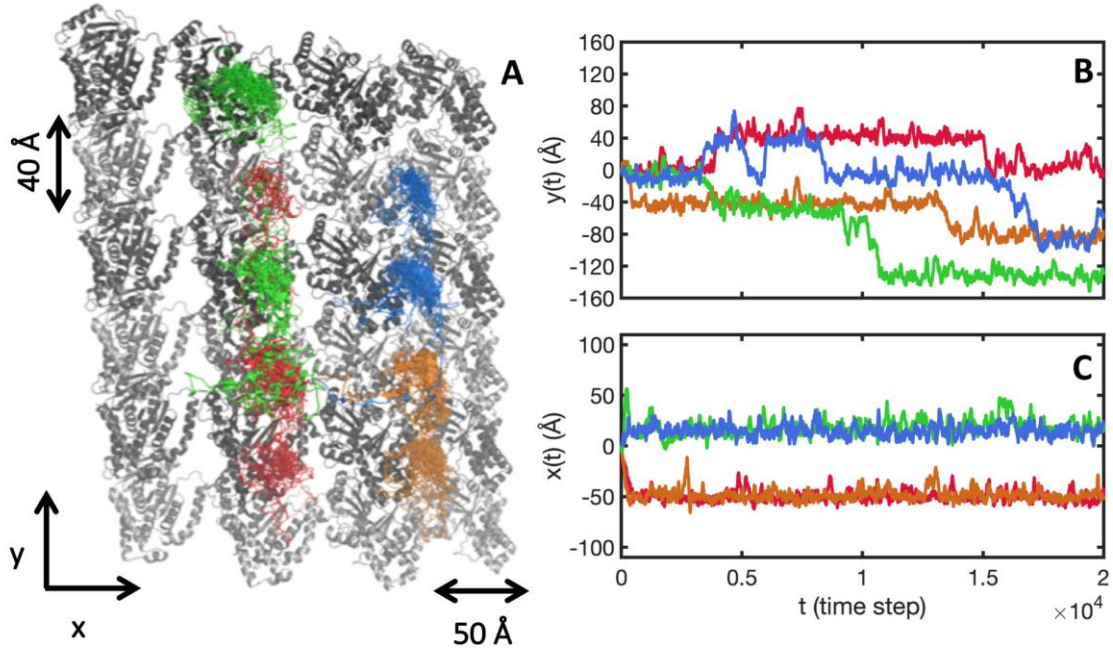

Figure S8. Trajectories of EB1 diffusing on MT with neutral tails. (A-C) same as in Fig. S7, but for MT with neutral tails.

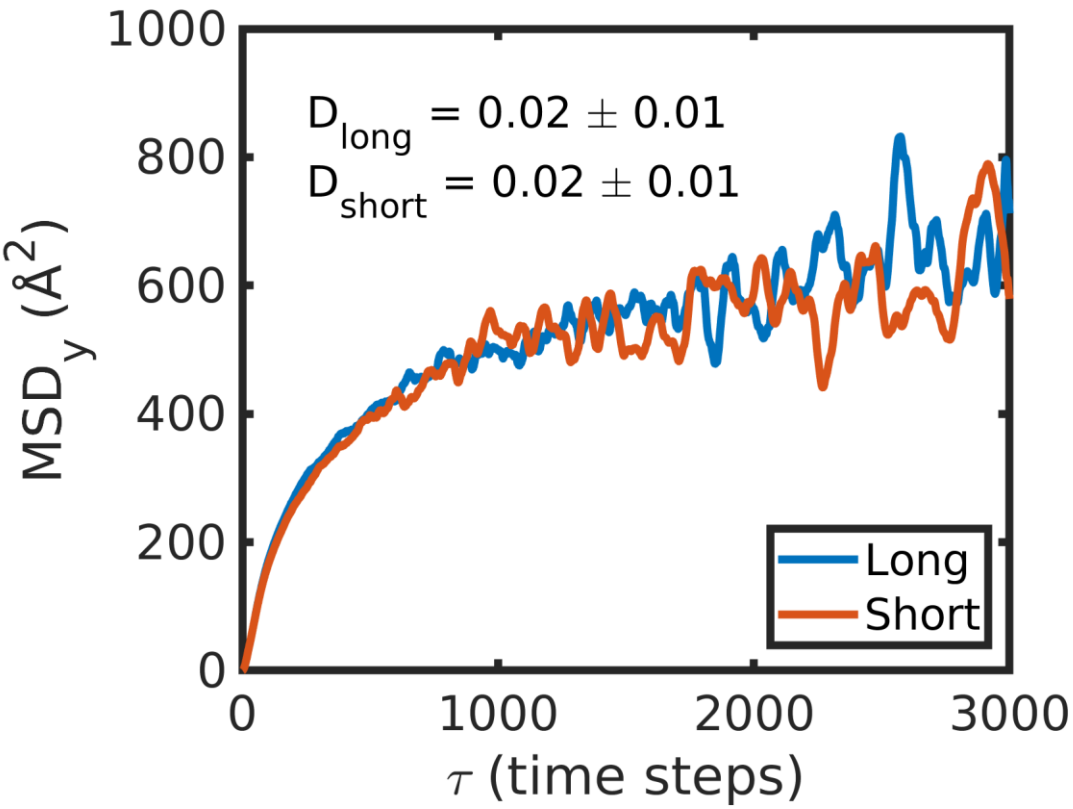

Figure S9. Comparison of MSD calculated from long and short simulations. In order to test if long simulations lead to improved sampling and better calculation of MSD, we preformed 5 simulations with $5*10^7$ steps (total $25*10^7$ time-steps), and compared them to 13 repeats of $2*10^7$ (total $26*10^7$ time-steps) which is the standard simulation length in this study. The blue line shows the MSD from the long simulations and the red line shoes the MSD from short simulations. The value of diffusion coefficients extracted from both simulations' lengths are similar, and so are the estimated errors from averaging several repeats.

Movie M1. EB1 diffusion on WT MT - CG MD.
Movie M2. EB1 diffusion on polyE MT - CG MD.
Movie M3. EB1 diffusion on MT without tails - CG MD.
Movie M4. EB1 diffusion on polyG MT - CG MD.
Movie M5. EB1 diffusion on WT MT - Atomistic MD.

References

1. Vemu A, et al. (2016) Structure and dynamics of single-isoform recombinant neuronal human tubulin. *J Biol Chem* 291(25):12907–12915.
2. Kellogg EH, et al. (2016) Near-atomic cryo-EM structure of PRC1 bound to the microtubule. *Proc Natl Acad Sci* 113(34):9430–9439.
3. Kellogg EH, et al. (2018) Near-atomic model of microtubule-tau interactions. *Science (80-)*:1–8.
4. Clementi C, Nymeyer H, Onuchic JN (2000) Topological and energetic factors: What determines the structural details of the transition state ensemble and "en-route" intermediates for protein folding? An investigation for small globular proteins. *J Mol Biol* 298(5):937–953.
5. Noel JK, Whitford PC, Sanbonmatsu KY, Onuchic JN (2010) SMOG@ctbp: Simplified deployment of structure-based models in GROMACS. *Nucleic Acids Res* 38(SUPPL. 2):W657–W661.
6. Noel JK, et al. (2016) SMOG 2: A Versatile Software Package for Generating Structure-Based Models. *PLoS Comput Biol* 12(3):e1004794.
7. Azia A, Levy Y (2009) Nonnative Electrostatic Interactions Can Modulate Protein Folding: Molecular Dynamics with a Grain of Salt. *J Mol Biol* 393(2):527–542.
8. Rüdiger M, Plessman U, Klöppel K-D, Wehland J, Weber K (1992) Class II tubulin, the major brain β tubulin isotype is polyglutamylated on glutamic acid residue 435. *FEBS Lett* 308(1):101–105.
9. Eddé B, et al. (1990) Posttranslational glutamylation of alpha-tubulin. *Science* 247(4938):83–5.
10. Westermann S, Weber K (2003) Post-translational modifications regulate microtubule function. *Nat Rev Mol Cell Biol* 4(12):938–947.
11. Sirajuddin M, Rice LM, Vale RD (2014) Regulation of microtubule motors by tubulin isotypes and post-translational modifications. *Nat Cell Biol* 16(4):335–344.
12. Pronk S, et al. (2013) GROMACS 4.5: A high-throughput and highly parallel open source molecular simulation toolkit. *Bioinformatics* 29(7):845–854.
13. Lindorff-Larsen K, et al. (2010) Improved side-chain torsion potentials for the Amber ff99SB protein force field. *Proteins Struct Funct Bioinforma* 78(8):1950–1958.
14. Hess B, Bekker H, Berendsen HJC, Fraaije JGEM (1997) LINCS: A Linear Constraint Solver for molecular simulations. *J Comput Chem* 18(12):1463–1472.
15. Bussi G, Donadio D, Parrinello M (2007) Canonical sampling through velocity

rescaling. *J Chem Phys* 126(1):014101.

16. Forth S, Hsia KC, Shimamoto Y, Kapoor TM (2014) Asymmetric friction of nonmotor MAPs can lead to their directional motion in active microtubule networks. *Cell* 157(2):420–432.
17. Hinrichs MH, et al. (2012) Tau protein diffuses along the microtubule lattice. *J Biol Chem* 287(46):38559–38568.
18. Baker NA, Sept D, Joseph S, Holst MJ, McCammon JA (2001) Electrostatics of nanosystems: Application to microtubules and the ribosome. *Proc Natl Acad Sci U S A* 98(18):10037–10041.